January, 1994

Improved Fokker–Planck model for the joint scalar, scalar gradient PDF

Rodney O. Fox, *Kansas State University*

Improved Fokker–Planck model for the joint scalar, scalar gradient PDF

R. O. Fox

Citation: Physics of Fluids (1994-present) **6**, 334 (1994); doi: 10.1063/1.868088
View online: http://dx.doi.org/10.1063/1.868088
View Table of Contents: http://scitation.aip.org/content/aip/journal/pof2/6/1?ver=pdfcov
Published by the AIP Publishing

Improved Fokker–Planck model for the joint scalar, scalar gradient PDF

R. O. Fox
College of Engineering, Kansas State University, Manhattan, Kansas 66506

(Received 27 February 1992; accepted 30 June 1993)

The joint scalar, scalar gradient probability density function (PDF) of an inert nonpremixed scalar diffusing in a one-dimensional system of random-sized lamellas is investigated by numerical simulation. The form of the scalar PDF, at a given RMS value, is nearly identical to that predicted by direct numerical simulation (DNS) of scalar mixing in isotropic turbulence and the mapping closure, and the moments of both the scalar and the scalar gradient suggest that their limiting marginal PDF are Gaussian. The joint scalar, scalar gradient PDF is found to be restricted to a bounded region in the scalar–scalar gradient plane, whose form is independent of the initial mixing ratio. These results are incorporated into the Fokker–Planck (FP) model for the joint scalar, scalar gradient PDF, and the improved model shows good agreement with numerical simulation data. An extension of the FP model that includes random stretching of the scalar gradient in isotropic turbulence is formulated.

I. INTRODUCTION

The probability density function (PDF) approach[1,2] is finding increased application in the computation of turbulent reactive flows.[3–6] One of the principal reasons behind this trend is the fact that, even for highly nonlinear reactions, the reaction rate expression appears in closed form in the PDF governing equation.[3] Nevertheless, the turbulent molecular mixing terms arising from diffusive terms in the fundamental balance equations must be closed. As has been noted elsewhere, these terms are dominated by the statistics of the scalar gradient.[7] Hence, greater knowledge of the form of the joint scalar, scalar gradient PDF is crucial in the development of adequate closures for turbulent molecular mixing.[7,8]

Experimental evidence for large Schmidt number turbulent flows[9–11] and direct numerical simulation (DNS) data[12] suggest that the bulk of the scalar dissipation occurs in a complex and highly intertwined set of layer-like structures.[9–11] These results further suggest the viability of nontraditional approaches for modeling the turbulent molecular mixing process such as the one-dimensional (1-D) linear eddy model[13] or the lamellar systems approach.[8,14–20] Following this line of reasoning, Fox[8,20] recently introduced the Fokker–Planck (FP) model for the joint scalar, scalar gradient PDF of *multiple, reactive* scalars derived based a simple physical model for scalar transport.

The FP model, unlike the mapping closure,[21] can be easily incorporated into the Monte Carlo algorithms employed for practical PDF computations.[2] Nonetheless, although the FP model predicts forms for the scalar PDF similar to those found by DNS of scalar mixing in isotropic turbulence[22] and by the mapping closure,[21,23] it was noted that DNS data for the joint scalar, scalar gradient PDF was needed to improve the model.[8] The goal of the present study is to use numerical simulation data for inert scalar diffusion in a 1-D lamellar system to further refine the FP model and to improve its ability to predict the evolution of the joint scalar, scalar gradient PDF.

Lamellar systems have been studied extensively by at least two groups. Muzzio *et al.*[14–16] have studied numerically systems of reactive lamellas, and found that the distribution of lamella thicknesses attains a self-similar form for almost all initial conditions. Sokolov and Blumen,[18,19] employing an analytical approach to study the same system, have derived conditions on the initial lamella thickness distribution that ensure self-similarity, and found an analytical expression for the self-similar lamella thickness distribution. Moreover, the latter two authors have invoked the central limit theorem to show that the limiting scalar PDF is Gaussian,[18] just as it is in the case of scalar mixing in isotropic turbulence.[22] This finding is confirmed in the present study, and, as expected, the *intermediate* forms of the scalar PDF are shown to be nearly identical to those found by DNS of scalar mixing in isotropic turbulence.[22]

The relevance of the pure diffusion case to turbulent scalar mixing studies has been pointed out by several authors.[24–26] For example, since pure diffusion represents an important limiting case, any viable molecular mixing closure should be able to predict the joint PDF in this limit. More compelling, however, is the fact that the mapping closure, which has been shown to yield excellent agreement with DNS data, is as equally applicable to one-dimensional (1-D) diffusion as it is to isotropic turbulence. The effect of latter enters the mapping closure through a time rescaling that leaves the form of the scalar PDF unchanged at a given RMS value.

Although no direct comparisons to isotropic turbulence DNS data are made in this study, an extension to the FP model to include the effect of turbulent stretching is proposed. Comparisons with turbulence DNS have been reported elsewhere,[27] with good agreement shown between the predicted scalar dissipation rate and the DNS data. Like in the mapping closure, the turbulent stretching term in the FP model primarily affects the rate of scalar dissipation and not the from of the marginal scalar PDF.

The remainder of this work is arranged as follows. In Sec. II, the original FP model is reviewed, an improved

 1070-6631/94/6(1)/334/15/$6.00

version is formulated, and an extension to include the effect of turbulent stretching is given. A discussion of the numerical approaches employed (numerical and Monte Carlo simulations) is provided in Sec. III. Section IV is devoted to the presentation and comparison of the numerical simulation data and FP model predictions for relevant statistical quantities, and for the marginal and joint PDF. Concluding remarks appear in Sec. V.

II. THE FOKKER–PLANCK MODEL

Using scalar mixing in lamellar structures as a paradigm for turbulent molecular mixing in general, Fox[20,8] has derived coefficients for the FP model for the joint scalar (ϕ), scalar gradient (Ψ) PDF. (Hereinafter, it will be assumed that the bounded scalar field has been rescaled so that $-1\leqslant\phi\leqslant 1$, and $\langle\phi^2\rangle$ and $\langle\psi^2\rangle$ will be used to denote the scalar variance and scalar gradient variance, respectively, even when the means $\langle\phi\rangle$ and $\langle\Psi\rangle$ are nonzero.) The FP model is expressed in terms of the normalized scalar (V) and the normalized magnitude of the scalar gradient (Z), defined by

$$V=\frac{\phi-\langle\phi\rangle}{\sqrt{\langle\phi^2\rangle}}=\frac{\phi-\langle\phi\rangle}{\phi'} \tag{1}$$

and

$$Z=\frac{|\Psi-\langle\Psi\rangle|}{\sqrt{\langle\psi^2\rangle}}=\frac{\psi}{\psi'}. \tag{2}$$

(For notational convenience, the magnitude of $\Psi-\langle\Psi\rangle$ will be denoted by ψ and referred to simply as the scalar gradient.)

As discussed in Sec. II D, models are required for the scalar RMS and the scalar gradient RMS, ϕ' and ψ', or, equivalently, for $\langle\phi^2\rangle$ and $\langle\psi^2\rangle$. Fox[8] has studied the properties of the FP model and shown, for example, that the limiting joint scalar, scalar gradient PDF is bivariate Gaussian, and that the scalar PDF evolves through forms similar to those seen in DNS[22] and the mapping closure.[23]

A. Original formulation

The original FP model is most easily expressed in terms of U and X, where $V=UX$ and $Z=U\sqrt{1-X^2}$. For a physical interpretation of these new variables, consider the simple case of equivolume mixing ($\langle\phi\rangle=0.0$) with a single length scale (e.g., lamella of equal thickness). For this case, let $\phi_{\max}(t)[=-\phi_{\min}(t)\leqslant 1]$ denote the maximum value of the scalar at time t, and define $X=\phi/\phi_{\max}$ and $U=\phi_{\max}/\phi'$. In the limit of large t, it is easily shown that, for this system,

$$\phi=\phi_{\max}(t)\sin(\pi x/L)=\phi_{\max}(t)X,$$

$$\psi=\frac{\pi}{L}\phi_{\max}(t)\cos\left(\frac{\pi x}{L}\right)=\frac{\pi}{L}\phi_{\max}(t)\sqrt{1-X^2},$$

where L is the lamella thickness. The definitions of V and Z in terms of U and X then follow. Note that for this case, U has a delta PDF (e.g., it is nonrandom), and

$$f_X(x)=\frac{1}{\pi\sqrt{1-x^2}}.$$

The joint PDF of V and Z is thus uniformly distributed on a unit circle in the V-Z plane.

In order to model the evolution of the joint PDF for the case of a distribution of length scales, Fox[8] proposed a bivariate FP equation,

$$\frac{\partial f_{U,X}}{\partial t}=-\frac{\partial}{\partial u}[A_U(u)f_{U,X}]+\frac{1}{2}\frac{\partial^2}{\partial u^2}[B_U(u)f_{U,X}]$$
$$-\frac{\partial}{\partial x}[A_X(x)f_{U,X}]+\frac{1}{2}\frac{\partial^2}{\partial x^2}[B_X(x)f_{U,X}]$$
$$+\frac{\partial^2}{\partial u\,\partial x}(B_{U,X}f_{U,X}),$$

with coefficients

$$A_U(u)=4\gamma\pi^2[(1/u)-u],$$

$$A_X(x)=-4\pi^2x,$$

$$B_U(u)=8\gamma\pi^2,$$

$$B_X(x)=8\pi^2(1-x^2),$$

and $B_{U,X}=0$, where γ is a model constant. U is now treated as a random variable, whose PDF is chosen so that the limiting joint PDF of V, and Z is bivariate Gaussian.

Despite the apparent good fit of the predicted scalar PDF to those produced by DNS, Fox[8] found that other statistics, such as the scalar variance dissipation correlation function, defined by

$$\rho=\langle V^2Z^2\rangle-1, \tag{3}$$

are poorly predicted by the model. These results can be improved considerably by modifying the coefficients as shown below to account for the form of the joint PDF at small t.

B. Improved FP model for equivolume mixing

The initial stages of mixing occur in noninteracting diffusion layers that are described by the well-known solution to the 1-D diffusion equation on an infinite interval:

$$\phi=\mathrm{erf}(\xi),\quad \xi=\frac{x}{\sqrt{4\,Dt}},$$

where D is the molecular diffusion coefficient. Note that this expression is independent of the lamella thickness; thus, it holds for both the single length scale and the distributed length scale cases. Using this result, one finds

$$\psi=\psi_{\max}(t)\exp[-(\mathrm{erf}^{-1}\,\phi)^2],$$

where $\psi_{\max}(t)=1/\sqrt{\pi\,Dt}$. Of greater interest, however, is the fact that this expression can be closely approximated by

$$\psi=\psi_{\max}(t)(1-\phi^2)^{\alpha},$$

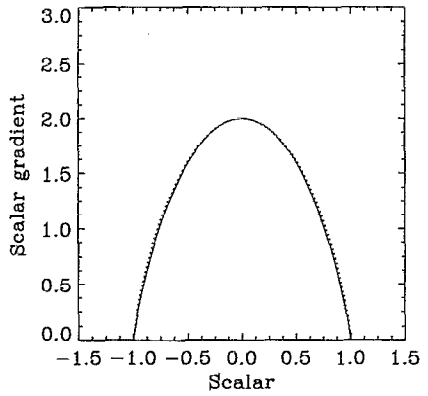

FIG. 1. Magnitude of the scalar gradient, ψ, versus scalar, ϕ. Solid line: $\psi=2\exp[-(\mathrm{erf}^{-1}\phi)^2]$. Dotted line: $\psi=2(1-\phi^2)^{0.8033}$.

where $\alpha=[1+\exp(-0.5)]/2\approx 0.8033$, as can be clearly seen in Fig. 1 [wherein $\psi_{\max}(t)=2.0$].

This result suggests that the scalar gradient can be closely approximated for all t by a function of the form

$$Y=\frac{\psi}{\psi_{\max}(t)}=(1-X^2)^{\alpha(\phi' U)},$$

with $\alpha(1)=[1+\exp(-0.5)]/2$ and $\alpha(x)\to 0.5$ as $x\to 0$ (i.e., the original model). Indeed, using the exact solution for the single length scale case, plots of $\ln Y$ vs $\ln(1-X^2)$ have been found to yield essentially straight lines. From the slopes of these lines at $\ln(1-X^2)=-1$ the following functional form has been found for $\alpha(x)$:

$$\alpha(x)=\tfrac{1}{2}(1+e^{-0.5x^{\gamma_e}}), \tag{4}$$

with $\gamma_e=26/3\approx 8.667$.

The improved FP model for equivolume mixing thus again treats U and X as random variables, but finds V and Z from

$$V=UX$$

and

$$Z=z_{\max}(t)[(\phi' U)^2(1-X^2)]^{\alpha(\phi' U)}.$$

In the latter expression, $z_{\max}(t)$ is a function that must be modeled. By definition, the maximum value of $\phi' U$ is unity and $\psi_{\max}$ occurs at $X=0$; hence

$$z_{\max}(t)=\frac{\psi_{\max}(t)}{\psi'(t)}. \tag{5}$$

A model for $\psi_{\max}$ that includes turbulent stretching is developed in Sec. II D.

Modified FP coefficients. The predictions of the FP model can be further improved by adopting the following modified FP coefficients:

$$A_U(u,t)=\kappa(t)\left(\frac{\gamma_1(t)}{u^2}-1\right)u,$$

$$A_X(x,u,t)=-\kappa(t)\gamma_1(t)\frac{x}{u^2},$$

$$B_U(u,t)=2\kappa(t)\gamma_2(t)[1-g_1(\phi' u)],$$

$$B_X(x,u,t)=2\kappa(t)\gamma_1(t)g_2(x,\phi' u,t)\frac{(1-x^2)}{u^2},$$

and $B_{U,X}=0$, where

$$g_1(x)=x^{\gamma_e} \tag{6}$$

and

$$\kappa(t)=\frac{D\langle\psi^2\rangle}{\langle\phi^2\rangle} \tag{7}$$

is the scalar dissipation rate. The functions $\gamma_1(t)$ and $\gamma_2(t)$ are found by forcing the second moments of V and Z to be unity. Likewise, g_2 is found by forcing the drift coefficient for Z to be linear.

The motivation for choosing these forms is as follows. First, as shown in Sec. IV, the joint scalar, scalar gradient PDF is bounded, implying that U is bounded. The function $g_1(\phi' u)$ is unity when ϕ attains it maximum or minimum value; hence B_U is null at the extremal values. Thus the random process for U has a natural boundary at $U=1/\phi'$.[28] The original FP model required the application of external boundary conditions. Second, both A_X and B_X have been modified by the factor $1/u^2$. This ensures that in the limit where $\phi'\to 0$, V, and Z will obey independent Ornstein–Uhlenbeck processes.[28] The joint PDF will then be independent, bivariate Gaussian, as seen in Sec. IV. Finally, the scalar dissipation rate, $\kappa(t)$, is the used as the inverse "correlation time" for scalar fluctuations. This is the "natural" choice, since it appears in the scalar variance decay equation (Sec. II D).

The functional form of g_2 is determined by requiring that the FP equation for Z have a drift coefficient, A_Z, linear in z and independent of v. For example, if g_2 is chosen to be

$$g_2(x,y,t)=\frac{1+(2\alpha-1)[\gamma_2(t)/\gamma_1(t)](1-x^2)[1-g_1(y)]}{1-(2\alpha-1)x^2}, \tag{8}$$

then treating α as constant and defining

$$h_1(t)=\frac{\psi_{\max}(\phi')^{2\alpha}}{\psi'}, \tag{9}$$

yields[29]

$$A_V(v,t)=-\kappa(t)v,$$

$$A_Z(z,t)=-[2\alpha\kappa(t)-\ln\dot{h}_1]z,$$

$$B_V(v,z,t)=2\kappa(t)\{\gamma_1(t)(1-x^2)g_2(x,\phi' u,t)+\gamma_2(t)x^2[1-g_1(\phi' u)]\},$$

$$B_Z(v,z,t)=8\alpha^2\kappa(t)\left(\gamma_1(t)\frac{z^2x^2g_2(x,\phi' u,t)}{u^2(1-x^2)}+\gamma_2(t)\frac{z^2}{u^2}[1-g_1(\phi' u)]\right),$$

and

$$B_{V,Z}(v,z,t)=4\alpha\kappa(t)\{\gamma_2(t)[1-g_1(\phi' u)]$$

$$-\gamma_1(t)g_2(x,\phi' u,t)\}\frac{vz}{u^2};$$

wherein u and x are implicit functions of v and z and $\ln \dot{h}_1$ is the time derivative of $\ln h_1$.

In the limit where $\alpha\to 0.5$ (i.e., as $\phi'\to 0$), $g_1(\phi' u)\to 0$, $g_2(x,y,t)\to 1$, and the FP coefficients become

$$A_V(v,t)=-\kappa(t)v,$$

$$A_Z(z,t)=-[\kappa(t)-\ln \dot{h}_1]z,$$

$$B_V(v,x,t)=2\kappa(t)[\gamma_1+(\gamma_2-\gamma_1)x^2],$$

$$B_Z(v,z,t)=2\kappa(t)[\gamma_2+(\gamma_1-\gamma_2)x^2],$$

and

$$B_{Z,V}=B_{V,Z}=2\kappa(t)(\gamma_2-\gamma_1)\frac{vz}{v^2+z^2}.$$

The functions $\gamma_1(t)$ and $\gamma_2(t)$ are determined by forcing both $\langle V^2\rangle$ and $\langle Z^2\rangle$ to be unity for all t. For the limiting case just considered where $\alpha=0.5$, $\langle Z^2 \ln \dot{h}_1\rangle\to 0$ (cf. Sec. II D); thus, these constraints yield $\gamma_1=\gamma_2=1$. The resultant FP equation then describes a bivariate, independent, Ornstein–Uhlenbeck process as noted earlier.

For the general case, a pair of linear equations in γ_1 and γ_2 results from

$$0=2\langle A_V(V,t)V\rangle+\langle B_V(V,Z,t)\rangle,$$

$$0=2\langle A_Z(Z,t)Z\rangle+\langle B_Z(V,Z,t)\rangle.$$

For example, the case where α is constant yields

$$\gamma_1(t)=\frac{(2\alpha\kappa-\langle Z^2 \ln \dot{h}_1\rangle)\beta_1-4\alpha^2\kappa\beta_3}{4\alpha^2\kappa(\beta_1\beta_4-\beta_2\beta_3)} \tag{10}$$

and

$$\gamma_2(t)=\frac{-(2\alpha\kappa-\langle Z^2 \ln \dot{h}_1\rangle)\beta_2+4\alpha^2\kappa\beta_4}{4\alpha^2\kappa(\beta_1\beta_4-\beta_2\beta_3)}, \tag{11}$$

where

$$\beta_1=\langle X^2[1-g_1(\phi' U)]\rangle,$$

$$\beta_2=\langle(1-X^2)g_2(X,\phi' U,t)\rangle,$$

$$\beta_3=\langle(Z^2/U^2)[1-g_1(\phi' U)]\rangle,$$

$$\beta_4=\left\langle\frac{Z^2X^2}{U^2(1-X^2)}g_2(X,\phi' U,t)\right\rangle.$$

C. Improved FP model for nonequivolume mixing

The nonequivolume mixing case ($\langle\phi\rangle\neq 0$) is initially (small t) very similar to the equivolume mixing case, since both can be approximated by diffusion layers. However, as time progresses, $\phi_{\max}(t)\neq-\phi_{\min}(t)$; thus, another variable in addition to U and X will be needed to describe ψ in terms of ϕ. Note that, by definition,

$$U=\frac{\phi_{\max}(t)-\phi_{\min}(t)}{2\phi'}.$$

We shall define the new variable ϕ^* by

$$\phi^*=\frac{\phi_{\max}(t)+\phi_{\min}(t)}{2}.$$

In the equivolume mixing case, $\phi^*=0$. Finally, we shall extend the definition of X to the present case by setting

$$X=\frac{\phi-\phi^*}{\phi' U}=\frac{V}{U}+\frac{\langle\phi\rangle-\phi^*}{\phi' U}.$$

For notational convenience, denote the conditional expectation of X given U by $\langle X|U\rangle$. Then, since $\langle V|U\rangle=0$,

$$V=U[X-\langle X|U\rangle];$$

hence

$$\langle X|U\rangle=\frac{\langle\phi\rangle-\phi^*}{\phi' U}. \tag{12}$$

Knowing ϕ^* for given $\phi' U$ and $\langle\phi\rangle$ is thus equivalent to knowing $\langle X|U\rangle$.

Study of the exact solution to the 1-D diffusion equation for the single length scale case reveals that ψ can be closely approximated by

$$\psi=\psi_{\max}(t)[\phi_{\max}(t)-\phi]^{\alpha_{\max}}[\phi-\phi_{\min}(t)]^{\alpha_{\min}},$$

where

$$\alpha_{\max}=\alpha\left(\frac{\phi' U}{1-\phi^*}\right) \tag{13}$$

and

$$\alpha_{\min}=\alpha\left(\frac{\phi' U}{1+\phi^*}\right). \tag{14}$$

Expressing Z in terms of U and X, the motivation for their new definitions becomes clear:

$$Z=z_{\max}(t)[\phi' U(1-X)]^{\alpha_{\max}}[\phi' U(1+X)]^{\alpha_{\min}},$$

i.e., this expression is identical to that used in the equivolume mixing case, where $\langle X|U\rangle=0$ and $\alpha_{\min}=\alpha_{\max}$. The FP coefficients given in Sec. II B should thus still be applicable after modifying A_X to account for $\langle X|U\rangle\neq 0$, as discussed below. A functional form is also be needed for $\langle X|U\rangle$.

The limiting values of ϕ^* are known: $\phi^*=0$ for $t=0$ ($\phi' U=1$), and $\phi^*\to\langle\phi\rangle$ for $t\to+\infty$ ($\phi' U\to 0$). In between, ϕ^* can be parametrized in terms of $\langle\phi\rangle$ and $\phi' U$, as shown in Fig. 2. Thus $\langle X|U\rangle$ can be treated as a known function of $\langle\phi\rangle$ and $\phi' U$. For example, for $\langle\phi\rangle=-0.5$, ϕ^* is closely approximated by

$$\phi^*(-0.5,\phi' U)=\frac{1+3(\phi' U)^4}{2[1+(\phi' U)^4]}-1.$$

For notational purposes, for fixed $\langle\phi\rangle$, define $h_2(s)=\langle X|\phi' U=s\rangle$ so that

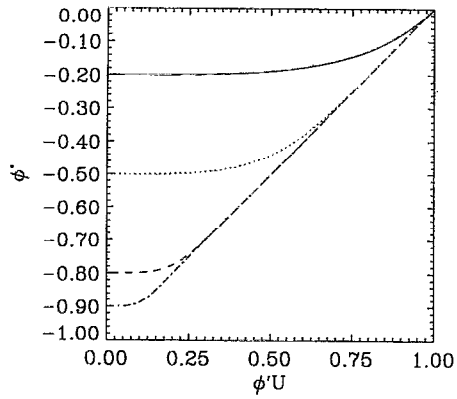

FIG. 2. Here ϕ^* vs $\phi' U$. Solid line: $\langle\phi\rangle=-0.2$. Dotted line: -0.5. Dashed line: -0.8. Dash–dotted line: -0.9.

$$h_2(s)=\frac{\langle\phi\rangle-\phi^*(\langle\phi\rangle,s)}{s}. \tag{15}$$

For the nonequivolume mixing case, $\langle X\,|\,U\rangle\neq 0$; thus A_X must be modified. Letting A_X have the form

$$A_X(x,u,t)=\kappa(t)\gamma_1(t)\frac{g_3(u,t)-x}{u^2}$$

the functional form of $g_3(u,t)$ can be found by forcing $A_V(v,t)=-\kappa(t)v$ as before. This yields

$$\begin{aligned} g_3(u,t)=&\left(1-\frac{2u^2}{\gamma_1(t)}\right)[h_2(\phi' u)+\phi' u\dot{h}_2(\phi' u)]\\ &+\frac{\gamma_2(t)}{\gamma_1(t)}\phi' u[\dot{h}_2(\phi' u)+\phi' u\ddot{h}_2(\phi' u)]\\ &\times[1-g_1(\phi' u)], \end{aligned} \tag{16}$$

wherein $\dot{h}_2$ and $\ddot{h}_2$ are the first and second derivatives of h_2, respectively.

The functional form of g_2 must be determined, as done in Sec. II B, by forcing $A_Z(z,t)$ to be linear in z and independent of v. Likewise, γ_1 and γ_2 will be modified by terms involving g_3.

D. Models for $\phi'(t)$, $\psi'(t)$, and $\psi_{\max}(t)$

In order to complete the FP model, functional forms are needed for $\phi'(t)$, $\psi'(t)$, and $\psi_{\max}(t)$. These will be derived for two cases: pure diffusion and isotropic turbulence. For both cases, the scalar variance ($\langle\phi^2\rangle=\phi'^2$) for an inert scalar can be found, given $\langle\psi^2\rangle$ from

$$\frac{d\langle\phi^2\rangle}{dt}=-2D\langle\psi^2\rangle=-2\kappa(t)\langle\phi^2\rangle. \tag{17}$$

Thus models are needed only for $\langle\psi^2\rangle$ and $\psi_{\max}$.

1. Pure diffusion

For this case, Sokolov and Blumen[18] have shown, based on the form of the Green's function solution to the 1-D diffusion equation, that in the limit of large t,

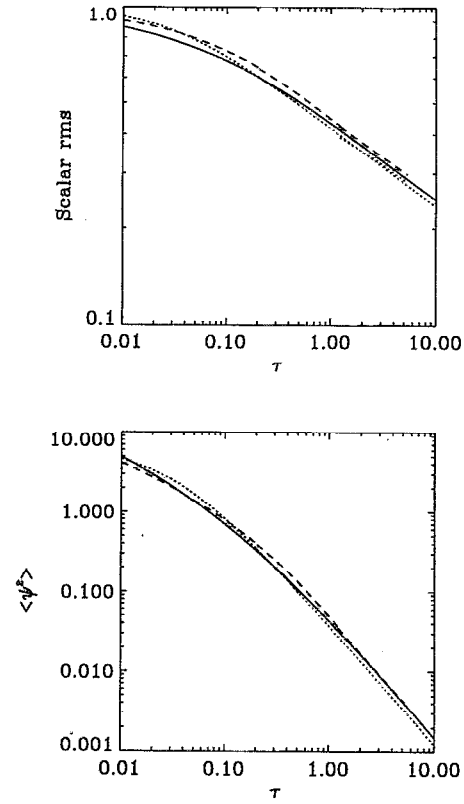

FIG. 3. Top: The evolution of the scalar RMS, ϕ', for 1-D diffusion equation. Bottom: The evolution of the $\langle\psi^2\rangle$. Solid line: Equivolume mixing. Dashed line: Nonequivolume mixing. Dotted line: FP model.

$$\langle\phi^2\rangle\to\frac{1}{\sqrt{Dt}}.$$

It follows from Eq. (17) that in the same limit,

$$\kappa(t)\to\frac{1}{4t}$$

or

$$\langle\psi^2\rangle\to\frac{1}{4\,Dt}\langle\phi^2\rangle.$$

Using these results, two possible models for $\langle\phi^2\rangle$ can be formulated.

First, using $\kappa(t)$ as the characteristic time for scalar gradient dissipation yields the following model for $\langle\psi^2\rangle$ for the pure diffusion case:

$$\frac{d\langle\psi^2\rangle}{dt}=-2C_\psi\kappa(t)\langle\psi^2\rangle, \tag{18}$$

where $C_\psi=3$ in the 1-D diffusion case. This model is compared with numerical simulation data in Fig. 3.

Alternatively, since $\langle\psi^4\rangle$ is closed in the PDF formulation, and, in the limit of large t, $\langle\psi^4\rangle\to 3\langle\psi^2\rangle^2$, $\langle\psi^2\rangle$ can be modeled by

$$\frac{d\langle\psi^2\rangle}{dt}=-2C_\psi^*\frac{\langle\psi^4\rangle}{\langle\phi^2\rangle},$$

where $C_\psi^* = 1$ in the 1-D diffusion case. The model constants can be determined for the 3-D diffusion case given knowledge of the limiting dependence of $\langle\psi^2\rangle$ on t.

As noted previously, $z_{\max}=\psi_{\max}/\psi'$. Thus, since ψ' can be found from Eq. (18), a model is needed for $\psi_{\max}$. For the pure diffusion case in the limit of large t, $D\psi_{\max}^2/\langle\phi^2(0)\rangle\to\kappa(t)\to 1/4t$. This behavior can be modeled by the following differential equation:

$$\frac{d\psi_{\max}}{dt}=-(C_\psi-1)\kappa_{\max}(t)\psi_{\max}, \tag{19}$$

where

$$\kappa_{\max}(t)=D\frac{\psi_{\max}^2}{\langle\phi^2(0)\rangle} \tag{20}$$

is a scalar dissipation rate based on the maximum scalar gradient. As noted earlier, this model should also apply to the 3-D diffusion case.

Notice that Eqs. (18) and (19) have the same form. Reformulating the models in terms of κ and $\kappa_{\max}$ yields identical expressions:

$$\frac{d\kappa}{dt}=-2(C_\psi-1)\kappa^2 \tag{21}$$

and

$$\frac{d\kappa_{\max}}{dt}=-2(C_\psi-1)\kappa_{\max}^2. \tag{22}$$

Using these expressions in Eq. (9) yields

$$\ln\dot{h}_1=(C_\psi-2\alpha)\kappa-(C_\psi-1)\kappa_{\max}.$$

Thus, $\ln\dot{h}_1\to 0$ in the limit where $\alpha\to 0.5$, so that $\langle Z^2\ln\dot{h}_1\rangle=\ln\dot{h}_1\to 0$, as stated earlier.

2. Isotropic turbulence

The mass conservation equation for a passive, inert scalar ϕ is

$$\frac{D\phi}{Dt}=D\frac{\partial^2\phi}{\partial x_i\,\partial x_i}.$$

From this expression, one finds the following equation the magnitude of the scalar gradient:

$$\frac{D\psi^2}{Dt}=2\,D\psi_i\frac{\partial^2\psi_i}{\partial x_j\,\partial x_j}-2\psi_i e_{ij}\psi_j,$$

where e_{ij} is the strain rate tensor. For isotropic turbulence, the first of these expressions yields Eq. (17),[2] while the second yields

$$\frac{d\langle\psi^2\rangle}{dt}=2D\langle\psi_i\nabla\psi_i\rangle-2\langle\psi_i e_{ij}\psi_j\rangle.$$

Neither of the terms on the right-hand side of this expression are closed. The first describes molecular mixing and the second, turbulent stretching of the gradient.

The gradient stretching term can be modeled by introducing the turbulence relaxation rate, $\omega(x,t)=\epsilon(x,t)/k(t)$, defined in terms of the pseudodissipation rate,

$$\epsilon(x,t)=\nu\frac{\partial u_i}{\partial x_j}\frac{\partial u_i}{\partial x_j},$$

where ν is the kinematic viscosity; and the turbulent kinetic energy, $k(t)$. Note that ϵ is a random variable, but k is not. Pope and Chen[30] have derived a stochastic model for ω that yields excellent agreement with DNS data. Their model is formulated in terms of an Ornstein–Uhlenbeck process for $\chi=\ln(\omega/\langle\omega\rangle)$ whose FP coefficients are

$$A_\chi(\chi,t)=\frac{1}{T_\chi}(\langle\chi\rangle-\chi),$$

$$B_\chi(t)=\frac{2\sigma^2(t)}{T_\chi},$$

where $\sigma^2(t)$ is the variance of χ and $T_\chi=1/C_\chi\langle\omega\rangle$ is an integral time scale.

In the FP model, the scalar gradient drift coefficient, A_ψ, will be extended to include gradient stretching by the addition of a bilinear term of the form $C_\omega\omega\psi$. Leaving the form of molecular mixing term unchanged, the models for the variances conditioned on the "stretching history," $\{\omega(s):0\leqslant s\leqslant t\}$, become

$$\frac{d\langle\phi^2\rangle_\omega}{dt}=-2\kappa_\omega\langle\phi^2\rangle_\omega \tag{23}$$

and

$$\frac{d\langle\psi^2\rangle_\omega}{dt}=-2C_\psi\kappa_\omega(t)\langle\psi^2\rangle_\omega+2C_\omega\omega(t)\langle\psi^2\rangle_\omega, \tag{24}$$

where $\kappa_\omega(t)=D\langle\psi^2\rangle_\omega/\langle\phi^2\rangle_\omega$. The unconditional variances, $\langle\phi^2\rangle$ and $\langle\psi^2\rangle$ can be found from the conditioned ones, $\langle\phi^2\rangle_\omega$ and $\langle\psi^2\rangle_\omega$, by averaging over the "stretching histories," $\{\omega(s):0\leqslant s\leqslant t\}$. Equation (18) for the pure diffusion case is recovered by setting $\omega(t)=0$.

Note that due to the appearance of the factor $\omega(t)\langle\psi^2\rangle_\omega$, correlations between ω and ψ can be important in determining the local mixing rate. The values of the model constants have been determined by Fox *et al.*[27] using DNS data for an isotropic initial scalar field in forced isotropic turbulence: $C_\psi=6.7$ and $C_\omega=4.7$.

Adding the gradient stretching term to Eq. (21), the model for κ_ω becomes

$$\frac{d\kappa_\omega}{dt}=2[C_\omega\omega(t)-(C_\psi-1)\kappa_\omega]\kappa_\omega. \tag{25}$$

This form is similar to one derived for $J\propto\sqrt{\kappa_\omega/D}$ by Gao[31] in his study of non-Gaussianity induced by random stretching in the mapping closure. In Gao's model, $\omega(t)$ in Eq. (25) is replaced by a Wiener process. Gao notes that J will be deterministic in the absence of turbulence ($\omega=0$), and lognormal in the absence of diffusion ($D=0$).

For the isotropic turbulence case, the FP model is expressed in terms of *conditional* normalized variables defined as in Eqs. (1) and (2), but with $\langle\phi^2\rangle_\omega$ and $\langle\psi^2\rangle_\omega$ used in place of $\langle\phi^2\rangle$ and $\langle\psi^2\rangle$, respectively. The FP coefficients given earlier are likewise modified by replacing $\kappa(t)$ with $\kappa_\omega(t)$. In the limit of large t, the conditional PDF for ϕ and ψ are thus again Gaussian, but with variances that

are "stretching history" dependent. The unconditional PDF can be found by averaging over the "stretching histories" and may exhibit non-Gaussian behavior.[31]

Isotropic turbulence will also affect $\kappa_{\max}$. This effect can be modeled by adding the gradient stretching term to Eq. (22):

$$\frac{d\kappa_{\max}}{dt}=2[C_\omega\omega(t)-(C_\psi-1)\kappa_{\max}]\kappa_{\max}. \tag{26}$$

The model for $\psi_{\max}$ follows from this expression

$$\frac{d\psi_{\max}}{dt}=[C_\omega\omega(t)-(C_\psi-1)\kappa_{\max}]\psi_{\max}. \tag{27}$$

Note that $\psi_{\max}$, like $\langle\phi^2\rangle_\omega$, is a random variable whose value again depends on the "stretching history" of the fluid particle. In particular, since ω can fluctuate to very large values, $\psi_{\max}$ at any t will have no upper bound, as is the case for pure diffusion (cf. Sec. IV C).

For the limiting case where ω can be treated as *time independent*, Eq. (25) yields the following expression for κ_ω in the limit of large t:

$$\kappa_\omega\to\frac{C_\omega}{C_\psi-1}\omega. \tag{28}$$

The limiting value of the unconditional scalar dissipation rate is then given by

$$\kappa_s=\frac{C_\omega}{C_\psi-1}\langle\omega\rangle.$$

The mechanical-to-scalar time-scale ratio[22,32] is thus $R=2\kappa_s/\langle\omega\rangle=2C_\omega/(C_\psi-1)=1.65$. This value is 50% smaller than the DNS value of 2.5.[22] The difference is due to the neglect of correlations between ψ and $\omega(t)$.

Defining the ratio of the scalar dissipation rate to its limiting value as κ_r, one finds

$$\frac{d\kappa_r}{dt}=2C_\omega\langle\omega\rangle(1-\kappa_r)\kappa_r,$$

which yields

$$\kappa_r(t)=\frac{\kappa_r(0)}{\kappa_r(0)+[1-\kappa_r(0)]e^{-2C_\omega\langle\omega\rangle t}}.$$

From this expression, it is clear that the scalar dissipation rate will approach its asymptotic value monotonely at a rate determined by $\langle\omega\rangle$. Moreover, if $\kappa_r(0)<1$, $\langle\psi^2\rangle$ will pass through a maximum at t^* found by solving $\kappa_r(t^*)=1-1/C_\psi$. However, if $\kappa_r(0)\geqslant 1$, $\langle\psi^2\rangle$ will decrease monotonely. This behavior is illustrated in Fig. 4. Such a dependence on initial conditions has been observed in DNS simulations.[22,33] Similar behavior should also be observed when $\langle\omega\rangle$ (but not ω) is time independent.

Finally, the unconditional limiting PDF of the scalar can be investigated for the case where ω is time independent. In the limit of large t, the conditional scalar is Gaussian with $\langle\phi^2\rangle_\omega=e^{-2C^*\omega t}$, where $C^*=C_\omega/(C_\psi-1)$. Moreover, defining the scaled even-order moments by

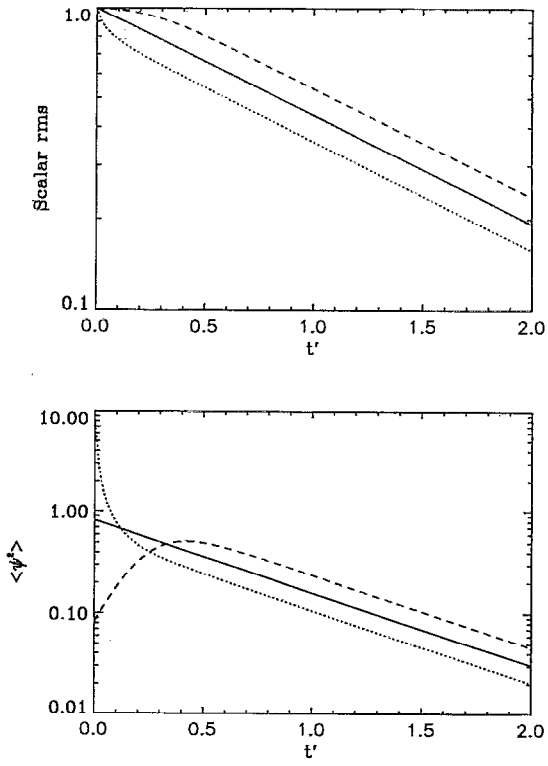

FIG. 4. Top: The evolution of the scalar RMS, ϕ', for isotropic turbulence with $t'=\langle\omega\rangle t$. Bottom: The evolution of the $\langle\psi^2\rangle$ for isotropic turbulence. Solid line: $\kappa_r(0)=1$. Dashed line: $\kappa_r(0)<1$. Dotted line: $\kappa_r(0)>1$.

$$F_{2n,\phi}=\frac{\langle\phi^{2n}\rangle}{\langle\phi^2\rangle^n},$$

it can easily be shown that

$$F_{2n,\phi}=\frac{(2n)!}{n!2^n}\frac{\langle e^{-2nC^*t\omega}\rangle}{\langle e^{-2C^*t\omega}\rangle^n}=\frac{(2n)!\Phi(ns)}{n!2^n\,\Phi(s)^n}\bigg|_{s=-2C^*t},$$

where $\Phi(s)$ is the moment generating function of ω.

As an example, consider the case where ω has a gamma distribution with mean $\langle\omega\rangle$ and parameter r:

$$f_\omega(\omega)=\frac{r^r}{\Gamma(r)}\frac{\omega^{r-1}}{\langle\omega\rangle^r}e^{-r\omega/\langle\omega\rangle}.$$

For this case, the moment generating function can be found analytically: $\Phi(s)=(1-\langle\omega\rangle s/r)^{-r}$. Thus, the scalar flatness factor is given by

$$F_{4,\phi}=3\frac{(1+2C^*\langle\omega\rangle t/r)^{2r}}{(1+4C^*\langle\omega\rangle t/r)^r},$$

and, in the zero-variance limit where $r\to+\infty$, the Gaussian value of 3 is obtained. For smaller values of r, the flatness factor will be larger than the Gaussian value. Gao[31] has derived a gamma PDF for ω and arrived at similar conclusions concerning the effect of turbulent stretching on the scalar PDF.

E. Time-dependent scalar bounds

A phenomena seen in DNS studies of scalar mixing noted by several authors[26,24,34] is the fact that the extremal values of the scalar field move toward the mean after a constant initial period. It is related to the largest length scale present in the DNS (both for pure diffusion and turbulence). As is obvious from the discussion in Sec. II B, the upper and lower bounds of the scalar field will be 1 and -1, respectively, only as long as lamella exist that are well described by a noninteracting diffusion layer approximation. Such lamella correspond to the largest structures in the initial scalar field, and their size is limited by the separation between the smallest resolvable scales and the largest scales in the simulation.

For mixing in real nonpremixed flows, where large-scale structures in the scalar field, can be on the order of millimeters or centimeters, the need for inclusion of this effect in the FP model is questionable. Nevertheless, it can be easily incorporated into the model by defining a time-dependent upper bound for $\phi' U$ [say $\mu(t)$], and replacing $g_1(\phi' u)$ with $g_1[\phi' u/\mu(t)]$. A model would then be needed for $\mu(t)$. For nonpremixed reactive flows in which reaction takes place in the nonpremixed state, the governing equation for μ would also need to include the effect of reaction.

F. Improved FP model for binary mixing

In summary, the improved FP model for a bounded scalar ($-1 \leqslant \phi \leqslant 1$) and its gradient for the mixing of two nonpremixed fluids is given by

$$\phi = \phi'_\omega V + \langle \phi \rangle, \tag{29}$$

$$\Psi = \psi \mathbf{r} + \langle \Psi \rangle, \tag{30}$$

$$\psi = \psi'_\omega Z, \tag{31}$$

$$V = U[X - \langle X | U \rangle], \tag{32}$$

$$Z = z_{\max}(t)[\phi'_\omega U(1-X)]^{\alpha_{\max}}[\phi'_\omega U(1+X)]^{\alpha_{\min}}, \tag{33}$$

where $\mathbf{r}$ is a isotropic random unit vector ($r_i r_i = 1$), and U and X obey a bivariate FP equation with coefficients

$$A_U(u,t) = \kappa_\omega(t)\left(\frac{\gamma_1(t)}{u^2} - 1\right)u, \tag{34}$$

$$A_X(x,u,t) = \kappa_\omega(t)\gamma_1(t)\frac{g_3(u,t) - x}{u^2}, \tag{35}$$

$$B_U(u,t) = 2\kappa_\omega(t)\gamma_2(t)[1 - g_1(\phi'_\omega u)], \tag{36}$$

$$B_X(x,u,t) = 2\kappa_\omega(t)\gamma_1(t)g_2(x,\phi'_\omega u,t)\frac{(1-x^2)}{u^2}, \tag{37}$$

$$B_{U,X} = 0. \tag{38}$$

The functions $\alpha_{\max}$, $\alpha_{\min}$, κ_ω, γ_1, γ_2, g_1, g_2, g_3, $\langle X | U \rangle$, and $z_{\max}$ are found, as described previously [Eqs. (4)–(16)]. The models for $\phi'_\omega(t)$, $\psi'_\omega(t)$, and $\psi_{\max}(t)$ are given in Sec. II D. Note that, unlike the original FP model (Sec. II A), the FP coefficients contain no model constants (i.e., γ). In addition to these expressions, the Pope and Chen stochastic model for ω[30] must be included for the case of isotropic turbulence.

III. NUMERICAL APPROACH

The validity of the improved FP model can be investigated by comparing the predicted joint scalar, scalar gradient PDF with ones generated by numerical simulation. The simplest test case is diffusion of a 1-D nonpremixed random scalar field. This case will be considered here. The case of scalar mixing in forced isotropic turbulence has been considered elsewhere.[27]

A. 1-D diffusion equation

The general solution to the 1-D diffusion equation on the unit interval can be expressed in terms of its Fourier transform coefficients.[18] However, in general, the lamella thickness, L, and its correlation with the scalar and scalar gradient are of interest for lamellar systems[8] and cannot be conveniently expressed in terms of the transformed solution. Thus, an explicit, constant-increment, finite-difference scheme[14] with periodic boundary conditions on the unit interval and $2^{20} = 1\,048\,576$ nodes has been used. The time step employed in the simulations is $\Delta\tau = (\Delta x)^2/6$, where $\Delta x = 2^{-7}$ and $\tau = Dt$. The scalar mean, $\langle \phi \rangle$, is a conserved quantity. Results for two cases will be presented here: equivolume mixing (i.e., Sec. II B), and nonequivolume mixing with $\langle \phi \rangle = -0.5$ (i.e., Sec. II C).

1. Initial conditions

The initial scalar field consisted of a series of up and down step functions between the values of -1 and $+1$. The spatial distance between each step was a random variable, whose mean value is the mean lamella thickness. For equivolume mixing, the initial random scalar field was generated using 2^{13} random integers between 0 and 2^{20} to fix the step locations. The random integers were computed from 2^{13} uniform random numbers by multipling them by 2^{20} and rounding to the nearest integer. It follows from the properties of the Poisson process that the distances between steps constructed in this manner were independent and exponentially distributed.

For nonequivolume mixing, the mean distance between steps for $\phi = -1$ was three times larger than for $\phi = +1$. The volume of fluid for which initially $\phi = -1$ was thus three times larger than the volume for which $\phi = +1$. Again, using 2^{13} random integers between 0 and 2^{20}, the step locations were determined for this case by letting the distance between two random integers represent the smaller volume, while the larger volume was represented by the distance up to the third random integer that followed. The latter, being sums of independent exponential random variables, are independent gamma random variables. This pattern was repeated until all 2^{13} random integers were exhausted. Note that in the nonequivolume mixing case the average lamella thickness is two times larger than in the equivolume mixing case.

2. Statistics and lamella depletion

For the results reported here, the lamella thickness is not a variable of interest and, thus, zero-crossing tracking algorithms will not be discussed. The PDF and relevant statistics have been estimated using ensemble averages based on samples of size 2^{15} randomly selected from the set of 2^{20} nodes at fixed time intervals. (There is little additional information that can be gained by using all 2^{20} nodes, since points at proximate spatial locations are highly correlated.) The scalar and its gradient at the sample nodes were the only output from the simulation. The scalar gradient has been computed from the scalar field using a first-order, finite-difference formula. The accuracy of the estimates of the moments and of the PDF depends strongly on the number of lamella used in the simulation and decreases with increasing time due to lamella depletion (i.e., the length scale increases with time resulting in a smaller effective sample as the spatial correlation increases).

In this study, the lamella number was initially very large (up to $2^{13}=8192$) and, hence, the time evolution of all statistics could be accurately computed without averaging over several runs. However, as is noted in Sec. IV C, when the scalar RMS value falls below approximately 0.35, the lamella number drops off quickly and the joint PDF show distinct traces of the underlying lamellar structure. Since it is ultimately related to the separation between the smallest resolvable scales and the largest scales in the simulation, this phenomena will also be present in the numerical simulation of the 3-D diffusion equation, such as those reported elsewhere.[25,26] It is avoided in forced isotropic turbulence simulations by the balancing effects of turbulent stretching (decreases length scales) and diffusion (increases length scales). One must therefore be careful when interpreting pure diffusion results for small values of the scalar RMS. Such results will only be significant when averaged over a large ensemble of simulations generated by independent initial scalar fields.

B. Monte Carlo simulation of the FP model

The Monte Carlo simulation of stochastic differential equations (SDEs) (e.g., Langevin equations) has been discussed extensively elsewhere.[2] The simulation of a FP equation proceeds analogously once it has been recast into the form of SDEs.[28,8] As seen in Sec. II F, the FP model is formulated in terms of a FP equation for U and X, wherein $B_{U,X}$ and $B_{X,U}$ are null. The corresponding SDEs are thus[28,29]

$$dU=A_U(u,t)dt+\sqrt{B_U(u,t)}dW_U(t),$$

$$dX=A_X(x,u,t)dt+\sqrt{B_X(x,u,t)}dW_X(t),$$

wherein W_U and W_X are independent Wiener processes.

The Monte Carlo simulation of the FP model has been carried out using a large number ($N=2^{15}=32{,}768$) notional particles. The numerical procedure involves six steps:

(1) Given ϕ and Ψ, find V and Z from Eqs. (1) and (2);

(2) using V and Z, invert Eqs. (32) and (33) to find U and X;

(3) Advance U and X according to their SDEs (Sec. II F);

(4) advance ϕ', ψ', and $\psi_{\max}$ according to their differential equations (Sec. II D);

(5) find V and Z, given U and X, from Eqs. (32) and (33);

(6) find ϕ and Ψ, given V and Z, from Eqs. (29)–(31).

The only steps that create potential difficulties are 2 and 3: step 2 because inverting Eq. (33) is nontrivial, and step (3) because the time-dependent functions appearing in the FP coefficients are complicated expected values of functions of U and X.

1. Implementation of step 2

Inversion of Eq. (33) is nontrivial for two reasons: when $\alpha_{\max}\neq\alpha_{\min}$, U can be found from V and Z only by a time-consuming numerical method; and even when $\alpha_{\max}=\alpha_{\min}$, these exponents are functions of U [Eqs. (13) and (14)]. These difficulties can be treated as follows.

(i) For nonequivolume mixing, replace $\alpha_{\max}$ and $\alpha_{\min}$ with $\alpha^*=\frac{1}{2}(\alpha_{\max}+\alpha_{\min})$ in Eq. (33), so that it becomes $Z=z_{\max}(t)[(\phi' U)^2(1-X^2)]^{\alpha^*(\phi' U)}$.

(ii) During one time step, treat $\phi' U$ in $\alpha^*(\phi' U)$ and $\phi^*(\langle\phi\rangle,\phi' U)$ as constant, i.e., $\alpha^*=\alpha^*[\phi' U(t)]=\alpha^*[\phi' U(t-dt)]$, and $v^*=U\langle X\,|\,U\rangle=(\langle\phi\rangle-\phi^*)/\phi'$ is constant.

Step 2 can then be carried out in closed form:

$$U=\sqrt{(V+v^*)^2+\frac{1}{\langle\phi^2\rangle}\left(\frac{Z}{z_{\max}(t)}\right)^{1/\alpha^*}}$$

and

$$X=\frac{V+v^*}{U}.$$

Note that, by definition, $U(0)=1$ and $\phi^*(0)=0$; thus, the numerical procedure is well defined.

2. Implementation of step 3

Although the time-dependent functions (γ_1, γ_2, and g_2) are well defined, they involve complicated expected values of U and X that quickly decay to their limiting values. In order to avoid computing these functions on every time step, two simplifications will be introduced: Set $g_2=1$ for all t; and set $\gamma_1(t)=\gamma_2(t)=1/[1-\langle X^2 g_1(\phi' U)\rangle]$, so that $\langle B_V\rangle=2\kappa(t)$. Recall that the values of these parameters were originally set to ensure that the the first two moments of V and Z remain constant. Thus, if these simplifications are employed, the moments must be verified, and, if needed, corrected on each time step.

3. Initial conditions

Initial values for ϕ and ψ have been generated by equally spaced samples (2^{15}) from the exact solution to the

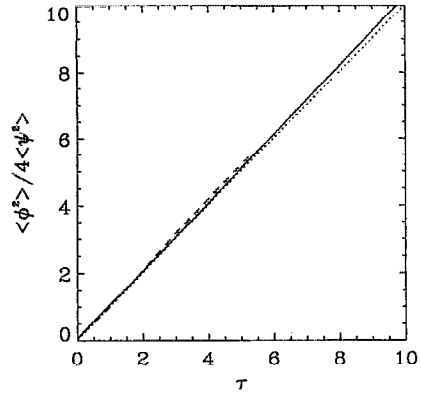

FIG. 5. The evolution of the $\langle\phi^2\rangle/4\langle\psi^2\rangle$ for the 1-D diffusion equation. Solid line: Equivolume mixing. Dashed line: Nonequivolume mixing. Dotted line: FP model.

1-D diffusion equation with periodic boundary conditions evaluated at $\tau = Dt = 10^{-4}$ ($\phi' = 0.984$ for the equivolume mixing case).

4. Isotropic turbulence

Although results for this case are not be presented here, the Monte Carlo simulation of isotropic turbulence proceeds as above, but with the addition of the SDE for ω given by Pope and Chen:[30]

$$d\omega = A_\omega(\omega,t) + \sqrt{B_\omega(\omega,t)}\,dW_\omega(t).$$

Thus each notional particle will carry with it random variables ϕ, ψ, and ω.

IV. MODEL VALIDATION

The improved FP model derived in Sec. II can be validated by comparing predicted statistics to the numerical results for the 1-D diffusion equation. Three types of predicted quantities will be compared: expected values such as ϕ', flatness factors, and superskewness; marginal PDF of ϕ and ψ; and the joint PDF of ϕ and ψ.

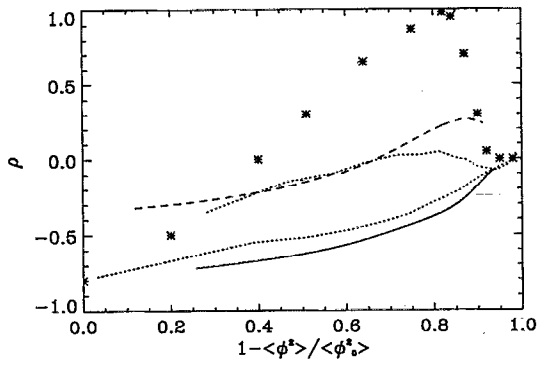

FIG. 6. The evolution of the scalar variance dissipation correlation function, ρ, for the 1-D diffusion equation. Solid line: Equivolume mixing. Dashed line: Nonequivolume mixing. Dotted lines: Improved FP model. Asterisk: Original FP model for the equivolume mixing case.

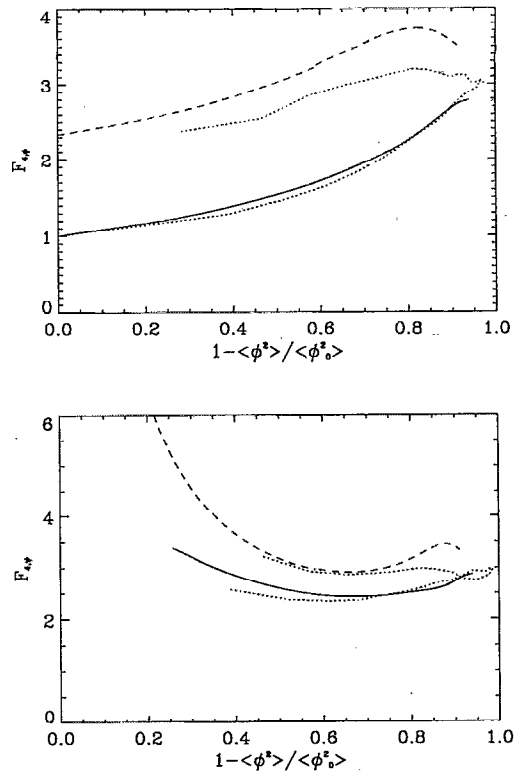

FIG. 7. Top: The evolution of the scalar flatness factor, $F_{4,\phi}$ for the 1-D diffusion equation. Bottom: The evolution of the scalar gradient flatness factor, $F_{4,\psi}$ for the 1-D diffusion equation. Solid line: Equivolume mixing. Dashed line: Nonequivolume mixing. Dotted lines: FP model.

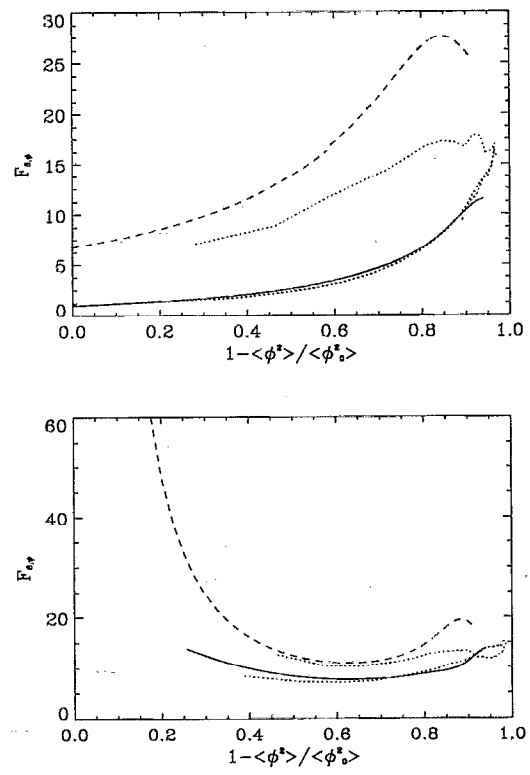

FIG. 8. Top: The evolution of the scalar flatness factor, $F_{6,\phi}$ for the 1-D diffusion equation. Bottom: The evolution of the scalar gradient flatness factor, $F_{6,\psi}$ for the 1-D diffusion equation. Solid line: Equivolume mixing. Dashed line: Nonequivolume mixing. Dotted lines: FP model.

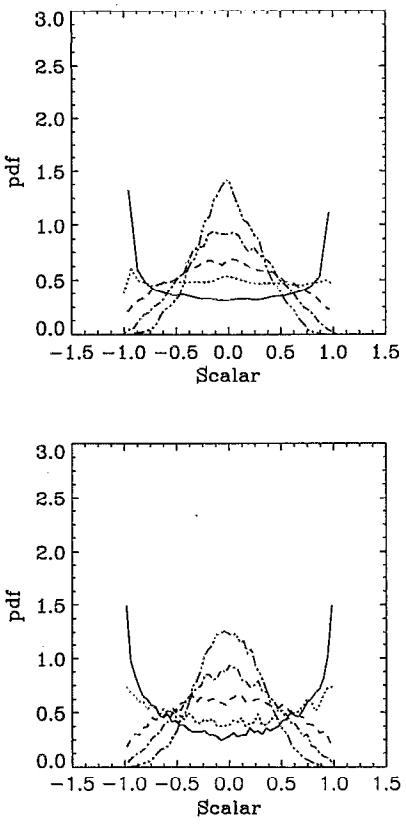

FIG. 9. The scalar PDF for the equivolume mixing case. Top: The 1-D diffusion equation at $\phi'=0.725$ (solid), 0.596 (dotted), 0.501 (dashed), 0.397 (dash–dot), and 0.301 (dash–dot–dot–dot). Bottom: FP model at $\phi'=0.693$ (solid), 0.623 (dotted), 0.507 (dashed), 0.413 (dash–dot), 0.304 (dash–dot–dot–dot).

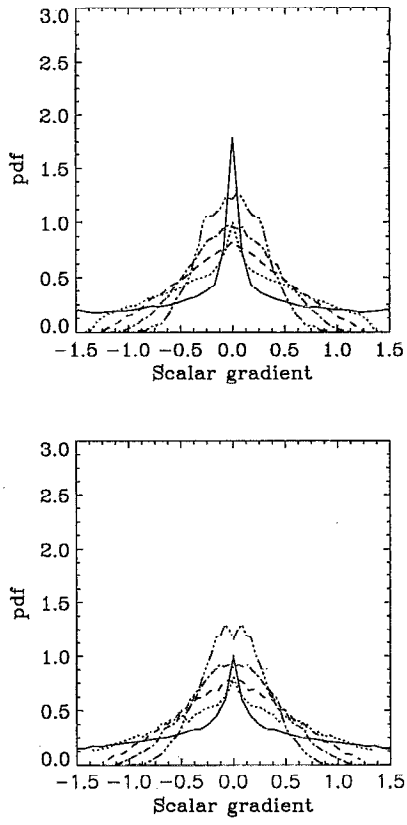

FIG. 10. The scalar gradient PDF for the equivolume mixing case. Top: The 1-D diffusion equation at $\phi'=0.725$ (solid), 0.596 (dotted), 0.501 (dashed), 0.397 (dash–dot), and 0.301 (dash–dot–dot–dot). Bottom: The FP model at $\phi'=0.693$ (solid), 0.623 (dotted), 0.507 (dashed), 0.413 (dash–dot), and 0.304 (dash–dot–dot–dot).

A. Expected values

Plots of scalar RMS (ϕ') vs $\tau=Dt$ from the 1-D diffusion equation are shown in Fig. 3. The FP model results found by solving Eqs. (17) and (18) are also shown. The model predictions are satisfactory both for small and large τ. Plots of $\langle\psi^2\rangle$ also show good agreement between the FP model and the 1-D diffusion equation. From Eq. (21) it can easily be shown that for large t, $\langle\phi^2\rangle/4\langle\psi^2\rangle\to Dt$ for the FP model. This is in good agreement with the 1-D diffusion equation (Fig. 5).

The scalar variance dissipation correlation function [Eq. (3)], ρ, is shown in Fig. 6. For the equivolume mixing case, the FP model slightly overpredicts the 1-D diffusion result; however, the rate of increase is well predicted. All the error is generated in the initial period, where the scalar dissipation rate is very large. For the nonequivolume mixing case, the FP model predictions are initially very good, but the agreement deteriorates as $\phi'\to 0$. This is due, at least in part, to the simplifications made in Sec. III C to simplify Eq. (33). In any case, the improved FP model's predictions of ρ are superior to the original model, as can be seen in Fig. 6.

The flatness factors for the scalar and the scalar gradient, defined, respectively, by

$$F_{4,\phi}=\frac{\langle(\phi-\langle\phi\rangle)^4\rangle}{\langle\phi^2\rangle^2}$$

and

$$F_{4,\psi}=\frac{\langle\psi^4\rangle}{\langle\psi^2\rangle^2},$$

are shown in Fig. 7. The FP model shows satisfactory agreement with the equivolume mixing case, but underpredicts $F_{4,\phi}$ for the nonequivolume mixing case. Note that all curves appear to be approaching the Gaussian limiting value of three.

Similar observations apply to the superskewness, defined by

$$F_{6,\phi}=\frac{\langle(\phi-\langle\phi\rangle)^6\rangle}{\langle\phi^2\rangle^3}$$

and

$$F_{6,\psi}=\frac{\langle\psi^6\rangle}{\langle\psi^2\rangle^3},$$

shown in Fig. 8. Here, the Gaussian limiting value is 15. The underpredictions in the nonequivolume mixing case are no doubt again due to the simplifications made in Sec. III B to allow the inversion of Eq. (33).

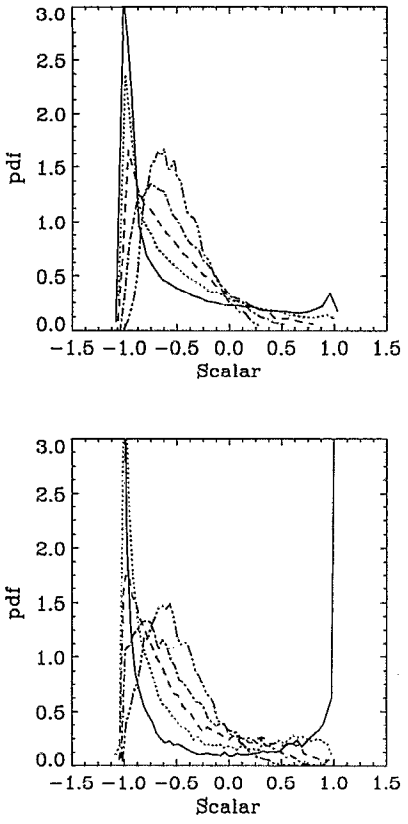

FIG. 11. The scalar PDF for the nonequivolume mixing case. Top: The 1-D diffusion equation at $\phi'=0.701$ (solid), 0.598 (dotted), 0.499 (dashed), 0.400 (dash–dot), and 0.300 (dash–dot–dot–dot). Bottom: The FP model at $\phi'=0.732$ (solid), 0.589 (dotted), 0.480 (dashed), 0.391 (dash–dot), and 0.288 (dash–dot–dot–dot).

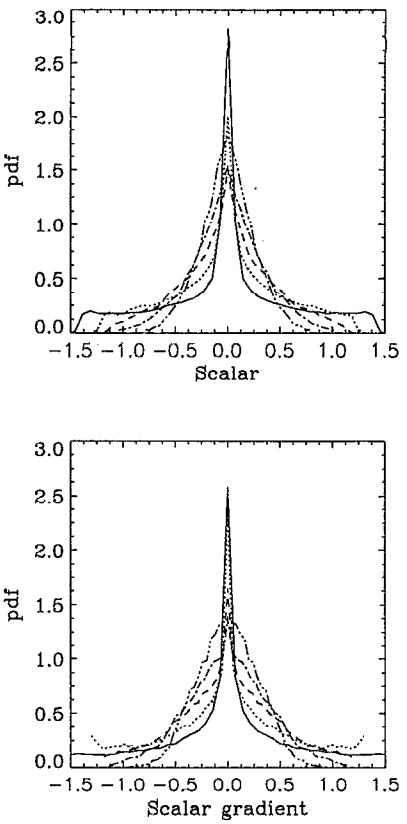

FIG. 12. The scalar gradient PDF for the nonequivolume mixing case. Top: The 1-D diffusion equation at $\phi'=0.701$ (solid), 0.598 (dotted), 0.499 (dashed), 0.400 (dash–dot), and 0.300 (dash–dot–dot–dot). Bottom: The FP model at $\phi'=0.732$ (solid), 0.589 (dotted), 0.480 (dashed), 0.391 (dash–dot), and 0.288 (dash–dot–dot–dot).

Similar comparisons of the higher-order scalar moments can be made with DNS data for isotropic turbulence. However, since extensive comparisons have been made elsewhere between the mapping closure and DNS, it suffices to note that the mapping closure is equally applicable to 1-D diffusion as it is to DNS. The good agreement between the mapping closure and DNS thus carries over to the 1-D diffusion equation results presented here when plotted in terms of the *scalar variance*. (This fact has been exploited by others for the 3-D diffusion case.[24]) The only quantities that will be very different in the isotropic turbulence case are the variances (cf. Fig. 3 and Fig. 4), and these control only the rate of "collapse" of the joint PDF but not its form.

B. Marginal PDF

The scalar PDF for equivolume mixing appear in Fig. 9 and the similarity between the 1-D diffusion equation and FP model results is remarkable. Moreover, as expected, both agree quite well with the mapping closure[23] and DNS.[22] Since the underlying physics is different in each case, the fact that all produce very similar scalar PDF suggests that the form is essentially controlled by the diffusion process. This is also the conclusion that Gao and O'Brien[7] arrived at for the cases of very large and very small Schmidt number based on time scales arguments.

The PDF of the scalar gradient, rescaled as $\psi^*=\psi\phi'/\psi'$, is shown in Fig. 10. It can be seen that initially the scalar gradient PDF is sharply peaked at the center, but that it also has extremely long tails. As time progresses, the scalar gradient PDF passes through a pyramidal shape (which corresponds to the inverted parabola shape for the scalar PDF) before moving toward a Gaussian form. Except for the height of the center peak during the initial period, this behavior is well predicted by the FP model.

The scalar PDF for nonequivolume mixing appear in Fig. 11 and the similarity between the 1-D diffusion equation and FP model results is again quite good, especially considering the simplifications introduced in Sec. III B. Similar remarks apply to the scalar gradient PDF shown in Fig. 12. The principal difference between the FP model and the 1-D diffusion equation is the behavior of the scalar PDF near the boundary at -1, where the model overpredicts the PDF. This overprediction leads to the underestimation of the flatness and superskewness, as seen in Figs. 7 and 8.

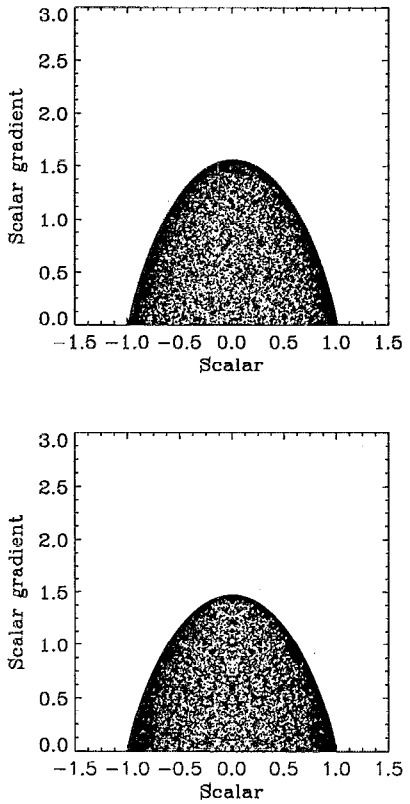

FIG. 13. Scatter plots of the scalar and the magnitude of the scalar gradient for the equivolume mixing case. Top: The 1-D diffusion equation at $\phi' = 0.725$. Bottom: The FP model at $\phi' = 0.693$.

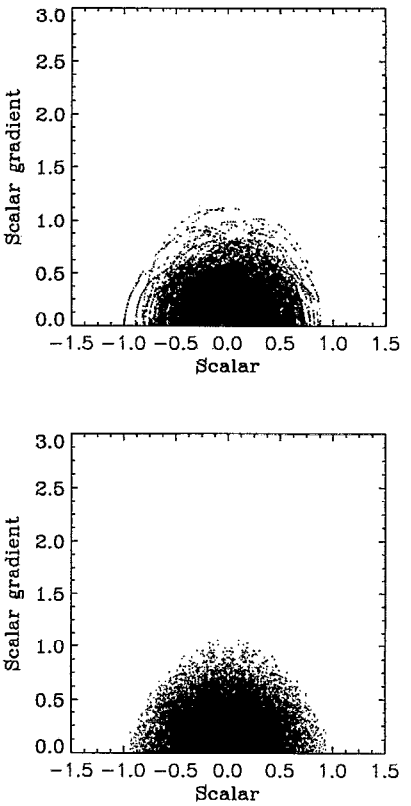

FIG. 14. Scatter plots of the scalar and the magnitude of the scalar gradient for the equivolume mixing case. Top: The 1-D diffusion equation at $\phi' = 0.301$. Bottom: The FP model at $\phi' = 0.304$.

C. Joint scalar, scalar gradient PDF

The number of data points available are insufficient to generate good estimates of the joint scalar, scalar gradient PDF. Instead, scatter plots of the scalar (ϕ) and the magnitude of the scalar gradient (ψ^*) for the equivolume mixing case are shown in Fig. 13 for $\phi' \approx 0.7$. Although it is not possible to directly compare the heights of the PDF in terms of the general shape of the support of the joint PDF, the agreement between the FP model and 1-D diffusion equation is excellent. As expected for the pure diffusion case, the scalar gradient is bounded above by $\psi_{\max}(1-\phi^2)^{0.8033}$ (cf. Fig. 1). In the initial stages, $\psi_{\max}$ is on the order of ψ' and thus has a strong effect on the shape of the joint PDF. The concentration of points near the upper boundary thus corresponds to fluid particles that are still well approximated by diffusion layers.

Scatter plots at a later time where $\phi' \approx 0.3$ are shown in Fig. 14. For this case, $\psi^*_{\max} = \psi_{\max}\phi'/\psi' \approx 1$, and thus has little effect on the shape of the joint PDF. Note, however, that the 1-D diffusion equation result now consists of many points lying on observable curves instead of randomly scattered points. This effect is due to lamella depletion and becomes more and more pronounced as ϕ' decreases.

Scatter plots for the nonequivolume mixing case are shown in Fig. 15 at $\phi' \approx 0.5$. The agreement between the FP model and 1-D diffusion equation is good, but not as good as in the equivolume mixing case. In particular, the model predicts a higher concentration of points near $(-1,0)$ than is seen with the 1-D diffusion equation. This is consistent with the results found for the marginal scalar PDF discussed above. Again, this discrepancy is no doubt due in large part to the simplification introduced in Sec. III B.

V. CONCLUSIONS

An improved formulation of the FP model governing the joint scalar, scalar gradient PDF has been derived and shown to agree well with numerical simulations for nonpremixed 1-D diffusion for the equivolume mixing case. The predicted evolution of the marginal and joint PDF show good agreement with the numerical simulation data. For the nonequivolume mixing case, the agreement was satisfactory, but not as good as in the equivolume mixing case, a fact due primarily to the simplification introduced in Sec. III B to make the model numerically tractable (i.e., setting $\alpha_{\max} = \alpha_{\min} = \alpha^*$). As pointed out in the Introduction, the pure diffusion case studied here is relevant to turbulent scalar mixing studies, both as a limiting case and due to the fact that the marginal scalar PDF is nearly the same for pure diffusion and for isotropic turbulence.

For binary mixing in the pure diffusion case, the joint PDF of the scalar and the magnitude of the scalar gradient is bounded above by a curve corresponding to a diffusion layer approximation. This boundary strongly affects the

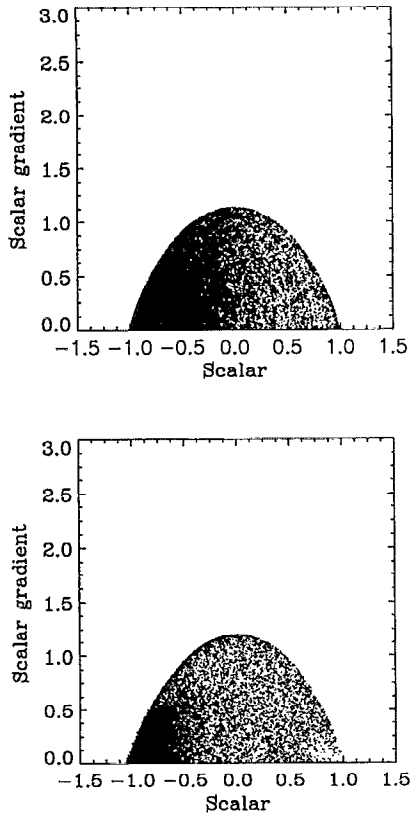

FIG. 15. Scatter plots of the scalar and the magnitude of the scalar gradient for the nonequivolume mixing case. Top: The 1-D diffusion equation at $\phi'=0.499$. Bottom: The FP model at $\phi'=0.480$.

initial form of the joint PDF. Its influence on the limiting form, however, is minimal and the joint scalar, scalar gradient PDF evolves toward a bivariate, independent Gaussian PDF for the pure diffusion case. Inclusion of this boundary for other initial conditions (e.g., mixing nonpremixed zones with more than two initial concentrations) in the pure diffusion case will be nontrivial, since it will be generated by the superposition of more than one diffusion layer.

The extension of the FP model to isotropic turbulence has been formulated and involves a random gradient stretching term in the scalar gradient drift coefficient. Initial comparisons of the FP model with forced isotropic turbulence DNS data has been presented elsewhere.[27] The additional gradient stretching term can lead to very large gradients. Thus, except near time zero, the joint scalar, scalar gradient PDF will not be bounded above in isotropic turbulence. Moreover, the difficulties noted above in the pure diffusion case associated with correct representation of the boundary should be mitigated by the lack of its importance in the isotropic turbulence case.

The ability of the FP model coupled with the Pope and Chen model for ω[30] to model DNS results for isotropic turbulence will be tested in future work. As discussed in Sec. III B, inclusion of the SDE for ω is straightforward, involving only the addition of a third random variable for each notional particle in the Monte Carlo simulation. However, for complete validation of the FP model, higher-resolution DNS data than is usually available will be needed in order to adequately resolve the three-variable joint PDF. (Fox *et al.*[27] have used 128^3 DNS to study two-variable joint PDF, but found three-variable PDF to be inadequately estimated at this resolution.)

Closing the PDF balance equation at the level of the scalar gradient allows for a direct treatment of the gradient stretching term. This is one of the primary motivations for formulating the FP model for the joint scalar, scalar gradient PDF instead of for only the scalar PDF. In comparison with turbulence moment closures, the FP model is thus analogous to a $k-\epsilon$ model, predicting both the scalar "kinetic energy" and the scalar dissipation rate. When the closed terms for chemical source terms are added, the FP model can be used to study the effect of reactions on the scalar microscale, which is an important parameter in nonpremixed combustion modeling.

In order to be useful for wide-scale application in pdf modeling of reactive flows, further work is needed to assess the FP model's ability to predict the joint scalar, scalar gradient PDF for more complex mixing cases. For example, cases that involve backmixing of partially mixed fluid will undoubtably require further modifications in the FP coefficients. In any case, given the acknowledged potential[2,3] of PDF methods for the computation of reactive flows in engineering and the key role played by turbulent molecular mixing models in their practical implementation, further research to develop improved mixing models should be vigorously pursued.

ACKNOWLEDGMENTS

This work has been supported by the National Science Foundation under Grant No. CTS-9158124 (PYI Award), the Donors of The Petroleum Research Fund (PRF No. 24807-G7E), administered by the American Chemical Society, and the Advanced Manufacturing Institute, Kansas State University (Project No. 92115). Numerical computations were carried out in part on the Cray Y-MP/48 system at the National Center for Supercomputing Applications, University of Illinois at Urbana—Champaign.

[1] E. E. O'Brien, in *Turbulent Reacting Flows*, edited by P. A. Libby and F. A. Williams (Springer-Verlag, New York, 1980).
[2] S. B. Pope, "PDF methods for turbulent reactive flows," Prog. Energy Combust. Sci. **11**, 119 (1985).
[3] S. B. Pope, "Computations of turbulent combustion: Progress and challenges," *23rd International Symposium on Combustion* (The Combustion Institute, Pittsburgh, 1990), pp. 591–612.
[4] D. Roekaerts, "Use of a Monte Carlo pdf method in a study of the influence of turbulent fluctuations on selectivity in a jet-stirred reactor," Appl. Sci. Res. **48**, 271 (1991).
[5] S. M. Correa and S. B. Pope, "Comparison of a Monte Carlo pdf/finite-volume model with bluff-body Raman data," *24th International Symposium on Combustion* (The Combustion Institute, Pittsburgh, 1992), pp. 279–285.
[6] R. O. Fox, "Computation of turbulent reactive flows: First-principles macro/micromixing models using probability density function methods," Chem. Eng. Sci. **47**, 2853 (1992).
[7] F. Gao and E. O'Brien, "Joint probability density function of a scalar and its gradient in isotropic turbulence," Phys. Fluids A **3**, 1625 (1991).
[8] R. O. Fox, "The Fokker–Planck closure for turbulent molecular mixing: Passive scalars," Phys. Fluids A **4**, 1230 (1992).

[9]W. J. A. Dahm and K. A. Buch, "High-resolution three-dimensional spatiotemporal measurements of the conserved scalar field in turbulent shear flows," in *Turbulent Shear Flows 7* (Springer-Verlag, Berlin, 1991).
[10]W. J. A. Dahm, K. B. Southerland, and K. A. Buch, "Four-dimensional laser induced fluorescence measurements of conserved scalar mixing in turbulent flows," in *Applications of Laser Techniques to Fluid Mechanics* (Springer-Verlag, Berlin, 1991).
[11]W. J. A. Dahm, K. B. Southerland, and K. A. Buch, "Direct, high resolution, four-dimensional measurements of the fine scale structure of $Sc \geq 1$ molecular mixing in turbulent flows," Phys. Fluids A **3**, 1115 (1991).
[12]G. R. Ruetsch and M. R. Maxey, "The evolution of small-scale structures in homogeneous isotropic turbulence," Phys. Fluids A **4**, 2747 (1992).
[13]A. R. Kerstein, "A linear-eddy model of turbulent scalar transport and mixing," Combust. Sci. Technol. **60**, 391 (1988).
[14]F. J. Muzzio and J. M. Ottino, "Evolution of a lamellar system with diffusion and reaction," Phys. Rev. Lett. **63**, 47 (1989).
[15]F. J. Muzzio and J. M. Ottino, "Dynamics of a lamellar system with diffusion and reaction: Scaling analysis and global kinetics," Phys. Rev. A **40**, 7182 (1989).
[16]F. J. Muzzio and J. M. Ottino, "Diffusion and reaction in a lamellar system: Self-similarity with finite rates of reaction," Phys. Rev. A **42**, 5873 (1990).
[17]F. J. Muzzio, P. D. Swanson, and J. M. Ottino, "The statistics of stretching and stirring in chaotic flows," Phys. Fluids A **3**, 822 (1991).
[18]I. M. Sokolov and A. Blumen, "Diffusion-controlled reactions in lamellar systems," Phys. Rev. A **43**, 2714 (1991).
[19]I. M. Sokolov and A. Blumen, "Distribution of striation thicknesses in reacting lamellar systems," Phys. Rev. A **43**, 6545 (1991).
[20]R. O. Fox, "A Fokker–Planck closure for turbulent molecular mixing in reactive flows," Bull. Am. Phys. Soc. **36**, 2684 (1991).
[21]S. B. Pope, "Mapping closures for turbulent mixing and reaction," Theor. Comput. Fluid Dyn. **2**, 255 (1991).
[22]V. Eswaran and S. B. Pope, "Direct numerical simulations of the turbulent mixing of a passive scalar," Phys. Fluids **31**, 506 (1988).
[23]L. Valino, J. Ros, and C. Dopazo, "Monte Carlo implementation and analytic solution of an inert-scalar turbulent-mixing test problem using a mapping closure," Phys. Fluids A **3**, 2191 (1991).
[24]T.-L. Jiang, P. Givi, and F. Gao, "Binary and trinary scalar mixing by Fickian diffusion—Some mapping closure results," Phys. Fluids A **4**, 1028 (1992).
[25]S. S. Girimaji, "On the modeling of scalar diffusion in isotropic turbulence," Phys. Fluids A **4**, 2529 (1992).
[26]S. S. Girimaji, "A mapping closure for turbulent scalar mixing using a time-evolving reference field," Phys. Fluids A **4**, 2875 (1992).
[27]R. O. Fox, J. C. Hill, F. Gao, R. D. Moser, and M. M. Rogers, "Stochastic modeling of turbulent reacting flows," in *Proceedings of the 1992 Summer Program* (Center for Turbulence Research, Stanford, 1992).
[28]C. W. Gardiner, *Handbook of Stochastic Methods* (Springer-Verlag, New York, 1983).
[29]H. Risken, *The Fokker–Planck Equation* (Springer-Verlag, New York, 1989).
[30]S. B. Pope and Y. L. Chen, "The velocity-dissipation probability density function model for turbulent flows," Phys. Fluids A **2**, 1437 (1990).
[31]F. Gao, "On the non-Gaussianity of scalar probability density function in homogeneous turbulence" (preprint, 1993).
[32]T.-L. Jiang and E. E. O'Brien, "Simulation of scalar mixing by stationary isotropic turbulence," Phys. Fluids A **3**, 1612 (1991).
[33]G. Kosaly, "Scalar mixing in isotropic turbulence," Phys. Fluids A **1**, 758 (1989).
[34]E. E. O'Brien and A. Sahay, "Asymptotic behavior of the amplitude mapping closure," Phys. Fluids A **4**, 1773 (1992).